


Nonperturbative simulation of anharmonic rattler dynamics in type-I clathrates with vibrational dynamical mean-field theory

Dipti Jasrasaria^{✉*} and Timothy C. Berkelbach^{✉†}

Department of Chemistry, Columbia University, New York, New York 10027, USA

 (Received 4 April 2024; revised 17 May 2024; accepted 30 July 2024; published 14 August 2024)

We use vibrational dynamical mean-field theory (VDMFT) to study the vibrational structure of type-I clathrate solids, specifically $X_8\text{Ga}_{16}\text{Ge}_{30}$, where $X = \text{Ba}, \text{Sr}$. These materials are cage-like chemical structures hosting loosely bound guest atoms, resulting in strong anharmonicity, short phonon lifetimes, and ultralow thermal conductivities. Presenting the methodological developments necessary for application to three-dimensional, atomistic materials, we validate our approach through comparison to molecular dynamics simulations and show that VDMFT is extremely accurate at a fraction of the cost. Through the use of nonperturbative methods, we find that anharmonicity is dominated by four-phonon and higher-order scattering processes, and it causes rattler modes to shift up in frequency by 50% (10 cm^{-1}) and to have lifetimes of less than 1 ps; this behavior is not captured by traditional perturbation theory. Furthermore, we analyze the phonon self-energy and find that anharmonicity mixes guest rattling modes and cage acoustic modes, significantly changing the character of the harmonic phonons.

DOI: [10.1103/PhysRevB.110.064312](https://doi.org/10.1103/PhysRevB.110.064312)

I. INTRODUCTION

Anharmonicity in the lattice vibrations of solids is responsible for temperature-dependent phonon frequency shifts and lifetimes, thermal expansion, and crystal structure stability [1]. A microscopic understanding of anharmonicity is essential for the emerging field of phononics, which aims to design and control the structural and dynamical properties of materials [2,3]. Examples include the engineering of materials with low thermal conductivities [4], which are important for thermal insulation or the generation of electricity from waste heat via thermoelectrics, or ultrafast optical control of lattice structure and dynamics [5]. From a theoretical perspective, the accurate description of anharmonicity requires the solution of a many-body problem, demanding the development of approximate numerical methods.

The simplest methods for describing anharmonicity are static mean-field theories, such as self-consistent phonon theory [6–10], which describe anharmonic systems using effective harmonic Hamiltonians with temperature-dependent frequencies. While these methods successfully predict some thermodynamic properties [11–15], they are not able to account for phonon lifetimes or non-QP (quasiparticle) effects. Perturbative methods can be used to calculate lifetimes due to phonon-phonon interactions [16–20], but they are often limited to lowest-order perturbation theory (PT) of three-phonon scattering processes and fail for systems with strong anharmonicity. Molecular dynamics (MD) simulations can describe anharmonic effects of classical nuclei exactly [18–23], but the computational cost associated with such direct simulation makes them expensive, especially for the

large system sizes necessary to eliminate finite-size effects; moreover, nuclear quantum dynamics can only be treated approximately [24].

In this paper, we apply the recently developed vibrational dynamical mean-field theory (VDMFT) [25], which is an extension of the successful DMFT for strongly correlated electrons [26–29]. VDMFT provides a nonperturbative description of local anharmonicity, and, as a Green's function theory, naturally yields both phonon frequency shifts and lifetimes. Here, we advance VDMFT by developing the methods necessary for application to three-dimensional atomistic solids with complex unit cells. We apply this method to study the anharmonic vibrational structure of clathrate solids, which are frameworks of covalently bonded atoms that host loosely bound “guest” atoms within their cage-like structures. The cage-guest interactions are strongly anharmonic, but their spatial locality makes these materials an ideal testbed for VDMFT.

We focus on the type-I clathrates $\text{Ba}_8\text{Ga}_{16}\text{Ge}_{30}$ (BaGG) and $\text{Sr}_8\text{Ga}_{16}\text{Ge}_{30}$ (SrGG), which have garnered much interest due to their ultralow thermal conductivities and promise for thermoelectric applications [30–40], as well as the fictitious empty clathrate $\text{Ga}_{16}\text{Ge}_{30}$ (GG). Theoretical and experimental studies of BaGG, SrGG, and related materials have revealed hybridization between acoustic modes of the cage lattice and optical, rattling modes of guest atoms, showing an avoided crossing in the harmonic dispersion relation [31,36,37] with potential implications for the thermal conductivity. While anharmonicity in these materials has been studied theoretically using analytical models [41,42], MD simulations [43,44], mean-field theory [37,40], and lowest-order PT [36–40], this work systematically examines anharmonicity with methods that go beyond conventional PT and/or static mean-field theory to determine the significance of nonperturbative effects.

*Contact author: dj2667@columbia.edu

†Contact author: t.berkelbach@columbia.edu

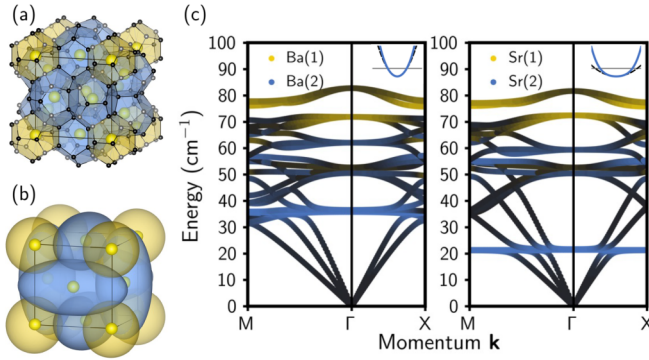


FIG. 1. (a) Crystal structure of BaGG [45], where Ba(1) atoms are in dodecahedral cages (gold) and Ba(2) atoms are in tetrakaidecahedral cages (blue). (b) Schematic of coarse-grained model of filled clathrates BaGG and SrGG, where the large cage atoms are colored according to their quartic cage-guest potentials. (c) Harmonic dispersion relations of BaGG (left) and SrGG (right), colored by their atomic character. The insets show the soft anharmonic interaction (blue line) between the $X(2)$ guest atoms and the 24-atom cages as well as the harmonic fitting (black dashed line) and value of $k_B T$ at 300 K (gray line).

We use VDMFT to calculate the anharmonic spectral functions of GG, BaGG, and SrGG at 300 K, and we find excellent agreement with those calculated from MD simulations at a fraction of the cost. Moreover, we find that lowest-order PT of three-phonon scattering processes fails to describe the short phonon lifetimes predicted by MD and VDMFT for the systems studied in this work. These comparisons validate VDMFT as an efficient and accurate method for describing anharmonicity in real materials beyond PT. While the vibrational structure of empty clathrates is relatively harmonic, our results show that anharmonicity significantly affects lattice dynamics of the filled clathrates studied here, especially SrGG. Guest-dominant phonon modes in particular show large frequency shifts, short lifetimes, and substantial mixing with cage-acoustic modes.

II. METHODS

A. Clathrate model

To study the vibrational structure of type-I clathrates, we first develop a coarse-grained model of the material, which is shown in Fig. 1. Because we are not interested in the high-frequency intracage dynamics nor the precise locations of the alloyed Ga and Ge atoms, we replace the clathrate cages by single “hollow” atoms. For simplicity, these cage atoms interact with one another through identical Lennard-Jones (LJ) potentials. To ensure the dynamical stability of the crystal, these unified cage atoms are arranged on an fcc lattice, which roughly approximates the positions of the atomistic clathrate cages. At each fcc site, guests are described by smaller atoms that interact with the cage atoms at those sites through anharmonic, quartic potentials. $X(1)$ guest atoms (where $X = \text{Ba, Sr}$) at the cube vertices interact via harder, isotropic potentials, representing interactions with the dodecahedral cages, while $X(2)$ guest atoms at the cube faces interact via softer, anisotropic potentials, mimicking the rattling

motions of guests in the tetrakaidecahedral cages [35]. Thus, a single unit cell in our model consists of eight atoms: four cage atoms and four guest atoms. The complete Hamiltonian for our clathrate model is given by

$$H = \frac{1}{2} \sum_{m\alpha} \left(\frac{p_{m\alpha}^2}{m_\alpha} \right) + \frac{1}{2} \sum_{m\alpha, n\beta}^{\text{cage}} V_{\text{LJ}}(|\mathbf{r}_{m\alpha} - \mathbf{r}_{n\beta}|) + \sum_m \sum_\alpha^{\text{cage}} \sum_\beta^{\text{guest}} V_q^{\alpha\beta}(\mathbf{r}_{m\alpha} - \mathbf{r}_{m\beta}), \quad (1)$$

$$V_{\text{LJ}}(r) = 4\epsilon \left[\left(\frac{\sigma}{r} \right)^{12} - \left(\frac{\sigma}{r} \right)^6 \right], \quad (2)$$

$$V_q^{\alpha\beta}(\mathbf{r}) = \sum_i \left(\frac{1}{2} K_{\beta,i} r_i^2 + g_{\beta,i} r_i^4 \right), \quad (3)$$

where the primed summation indicates that only cages and guests on the same lattice site interact. Here, \mathbf{m}, \mathbf{n} are lattice translation vectors, α, β are indices over atoms in the unit cell, and i is an index over the Cartesian directions. The position, momentum, and mass of atom α in cell \mathbf{m} are given by $\mathbf{r}_{m\alpha}$, $\mathbf{p}_{m\alpha}$, and m_α , respectively.

To parametrize the above Hamiltonian, we fit the LJ parameters and the harmonic frequencies, $K_{\alpha,i}$, of the cage-guest interactions to reproduce the harmonic dispersion relations from *ab initio* calculations [36,37,40]. The harmonic dispersion relation is obtained through diagonalization of the dynamical matrix,

$$\mathcal{D}_{\alpha i, \beta j}(\mathbf{k}) = \frac{1}{\sqrt{m_\alpha m_\beta}} \sum_m e^{i\mathbf{k} \cdot (\mathbf{R}_{m\alpha} - \mathbf{R}_{0\beta})} \frac{\partial^2 \mathcal{V}}{\partial u_{m\alpha i} \partial u_{0\beta j}}, \quad (4)$$

where \mathbf{k} is a wave vector in the first Brillouin zone (BZ), and $\mathbf{R}_{m\alpha}$ is the equilibrium position of atom α in cell \mathbf{m} . The derivative of the lattice potential, \mathcal{V} , with respect to atomic displacements, $u_{m\alpha i} = r_{m\alpha i} - R_{m\alpha i}$, is evaluated at the equilibrium lattice configuration. The dynamical matrix defines the harmonic phonon modes,

$$u_\lambda(\mathbf{k}) = N^{-1/2} \sum_{m\alpha i} c_{\alpha i, \lambda}(\mathbf{k}) e^{-i\mathbf{k} \cdot \mathbf{R}_{m\alpha}} \sqrt{m_\alpha} u_{m\alpha i}, \quad (5)$$

where $\mathbf{c}(\mathbf{k})$ are the eigenvectors of $\mathcal{D}(\mathbf{k})$.

The harmonic dispersion relations of our model BaGG and SrGG are illustrated in Fig. 1(c). The low-frequency rattling motions of $X(2)$ guest atoms lead to flat modes that cut through the acoustic branches of the cage lattice, leading to the hallmark avoided crossing of these materials. Vibrations of the $X(1)$ guest atoms are higher in frequency, hybridizing with the optical modes of the cage lattice. We complete the parametrization of our Hamiltonian by choosing the quartic anharmonicity parameters $g_{\alpha,i}$ in Eq. (3) to reproduce the behavior of *ab initio* cage-guest potential energy surfaces for guest atoms Ba and Sr [32,40]. Complete details of our clathrate model and further discussion are given in the Supplemental Material (SM) [46].

B. Anharmonic lattice dynamics

To compute the anharmonic lattice dynamics of the clathrate model defined above, we use vibrational dynami-

cal mean-field theory (VDMFT). In VDMFT, we compute the anharmonic phonon Green's function (GF) [1,51] of the periodic lattice, $\mathbf{D}(\mathbf{k}, \omega)$, which encodes phonon frequencies and lifetimes. The spectral part of the GF is experimentally measurable by inelastic neutron scattering, and computationally, the GF can be used to calculate one-body averages and approximations to thermal conductivities. Although VDMFT can treat quantum or classical nuclei [25], here we use classical dynamics, as nuclear quantum effects are unimportant for these clathrates at room temperature. Thus, the classical GF is

$$\mathbf{D}(\mathbf{k}, t) = \frac{\theta(t)}{k_B T} \langle \dot{\mathbf{u}}(\mathbf{k}, t) \mathbf{u}^T(-\mathbf{k}, 0) \rangle, \quad (6)$$

where \mathbf{D} is a matrix, \mathbf{u} is a column vector, and $\langle \cdot \rangle$ indicates an equilibrium average at temperature T . The Fourier transform of the GF satisfies a Dyson equation,

$$\mathbf{D}^{-1}(\mathbf{k}, \omega) = \mathbf{D}_0^{-1}(\mathbf{k}, \omega) - 2\mathbf{\Omega}(\mathbf{k})\boldsymbol{\pi}(\mathbf{k}, \omega), \quad (7)$$

where $\mathbf{D}_0(\mathbf{k}, \omega) = [\omega^2 \mathbf{1} - \mathbf{\Omega}^2(\mathbf{k})]^{-1}$ is the GF of the harmonic lattice, $\mathbf{\Omega}^2(\mathbf{k})$ is the dynamical matrix [so that $\mathbf{\Omega}^2(\mathbf{k}) = \mathcal{D}(\mathbf{k})$ in the atomic basis], and $\boldsymbol{\pi}(\mathbf{k}, \omega)$ is the self-energy that describes anharmonicity in the lattice. VDMFT makes the approximation of a local self-energy, $\boldsymbol{\pi}(\mathbf{k}, \omega) \approx \boldsymbol{\pi}(\omega)$, which we calculate nonperturbatively by solving a so-called impurity problem. Specifically, VDMFT maps the problem of a periodic lattice onto that of a single unit cell (the ‘‘system’’) interacting with a fictitious bath of harmonic oscillators characterized by a tailored spectral density [25–27]. This impurity problem is generally easier to solve than the full periodic problem because of the small number of degrees of freedom in the finite system.

The unit cell atoms that constitute the system experience a local, anharmonic, many-body potential $V_{\text{loc}}(\mathbf{u})$ and the GF that describes the isolated system is given by $\mathbf{D}_{\text{sys}}(\omega) = [\omega^2 \mathbf{1} - \mathbf{\Omega}^2 - 2\mathbf{\Omega}\boldsymbol{\pi}(\omega)]^{-1}$, where $\mathbf{\Omega}^2$ is the system dynamical matrix with respect to $V_{\text{loc}}(\mathbf{u})$. The harmonic bath and system-bath coupling are determined by the hybridization $\mathbf{\Delta}(\omega)$, which describes the effect of the lattice on the dynamics of the isolated system,

$$-2\mathbf{\Omega}\mathbf{\Delta}(\omega) = \mathbf{D}_C^{-1}(\omega) - \mathbf{D}_{\text{sys}}^{-1}(\omega), \quad (8)$$

where $\mathbf{D}_C(\omega) = N_k^{-1} \sum_{\mathbf{k}} \mathbf{D}(\mathbf{k}, \omega)$ is the cellular GF, and N_k is the number of points sampled in the BZ. Details regarding the definition of the impurity problem, including $V_{\text{loc}}(\mathbf{u})$, are given in the SM [46].

The (classical) dynamics of the system coordinates are governed by a set of coupled generalized Langevin equations (GLEs),

$$\ddot{\mathbf{u}}(t) = -\nabla V_{\text{eff}}(\mathbf{u}) - \int_0^t ds \boldsymbol{\gamma}(t-s) \dot{\mathbf{u}}(s) + \boldsymbol{\xi}(t). \quad (9)$$

Here, $\boldsymbol{\gamma}(t)$ is a matrix of friction kernels that describes the dissipative effect of the bath on the system dynamics and is related to the hybridization,

$$\boldsymbol{\gamma}(t) = -2\sqrt{\frac{2}{\pi}} \int_0^\infty d\omega \cos(\omega t) \frac{2\mathbf{\Omega} \text{Im} \mathbf{\Delta}(\omega)}{\omega}, \quad (10)$$

where $\text{Im}(\cdot)$ denotes the imaginary part. The effective potential $V_{\text{eff}}(\mathbf{u})$ includes the bath-induced renormalization of

the local potential, and $\boldsymbol{\xi}(t)$ is a vector of random forces that satisfies the fluctuation-dissipation relation $\langle \boldsymbol{\xi}(t) \boldsymbol{\xi}^T(s) \rangle = k_B T \boldsymbol{\gamma}(t-s)$.

As detailed in the SM [46], with thermal sampling of the initial conditions, the above GLEs are solved numerically [52,53] to obtain dynamics of the system coupled to the bath and to compute the anharmonic impurity GF, $\mathbf{D}_{\text{imp}}(t) = (k_B T)^{-1} \theta(t) \langle \dot{\mathbf{u}}(t) \mathbf{u}^T(0) \rangle$. From this, the self-energy is obtained as

$$\boldsymbol{\pi}(\omega) = \frac{1}{2} \mathbf{\Omega}^{-1} [\mathbf{D}_{\text{imp},0}^{-1}(\omega) - \mathbf{D}_{\text{imp}}^{-1}(\omega)], \quad (11)$$

where $\mathbf{D}_{\text{imp},0}(\omega)$ is the harmonic impurity GF. This local self-energy is used to calculate the lattice GF [i.e., Eq. (7) with the impurity $\boldsymbol{\pi}(\omega)$ in place of $\boldsymbol{\pi}(\mathbf{k}, \omega)$], leading to an iterative procedure that converges once the self-consistency condition $\mathbf{D}_C(\omega) = \mathbf{D}_{\text{imp}}(\omega)$ has been reached. For the systems studied here, we find that self-consistency is achieved in one iteration, as shown in the SM [46].

Due to the sampling of initial conditions, the calculated impurity GFs have statistical noise, leading to issues of noncausality and negative spectral functions (see SM [46]). Furthermore, converging the numerical Fourier transform requires the propagation of long trajectories. Therefore, instead of numerically Fourier transforming $\mathbf{D}_{\text{imp}}(t)$, we fit its elements to the functional form of the GF of a damped harmonic oscillator and perform the Fourier transform analytically. This fitting technique, which is further described in the SM [46], circumvents the need to run many long trajectories—making our approach significantly more efficient while retaining excellent frequency resolution—and ensures a causal self-energy through simple constraints on the fitting parameters.

III. RESULTS AND DISCUSSION

We use VDMFT to calculate the anharmonic GF and spectral function, $A(\mathbf{k}, \omega) = -\pi^{-1} \text{Tr}[\text{Im} \mathbf{D}(\mathbf{k}, \omega)]$, of GG, BaGG, and SrGG at 300 K, which are illustrated in Fig. 2. While the empty GG clathrate is largely harmonic, the filled clathrates feature anharmonicity that causes peaks to shift to energies higher than those predicted by the harmonic dispersion relation and causes them to broaden due to phonon scattering. Interestingly, anharmonicity affects modes differently; while the cage-dominant acoustic modes remain relatively unchanged from their harmonic dispersion, modes with an appreciable guest character show large effects. In particular, the flat Ba(2) rattling modes shift from 36 to 39 cm^{-1} , and the Sr(2) rattling modes, which have lower harmonic frequencies and stronger quartic anharmonicity, shift from 21 to 33 cm^{-1} and acquire a linewidth of 8 cm^{-1} , which corresponds to a short lifetime of 0.67 ps. The hardening of these rattling modes also affects the avoided crossing with the cage acoustic modes. In the SM [46], we present the temperature dependence of the VDMFT spectral function of SrGG from 50 to 600 K, showing that the Sr(2) rattling mode significantly broadens and hardens with increasing temperature.

To evaluate the accuracy of VDMFT, we compare to the exact spectral function computed using MD simulations of a large supercell with periodic boundary conditions (MD simulation details are given in the SM [46]). Figures 2 and 3 demonstrate that agreement between VDMFT and MD

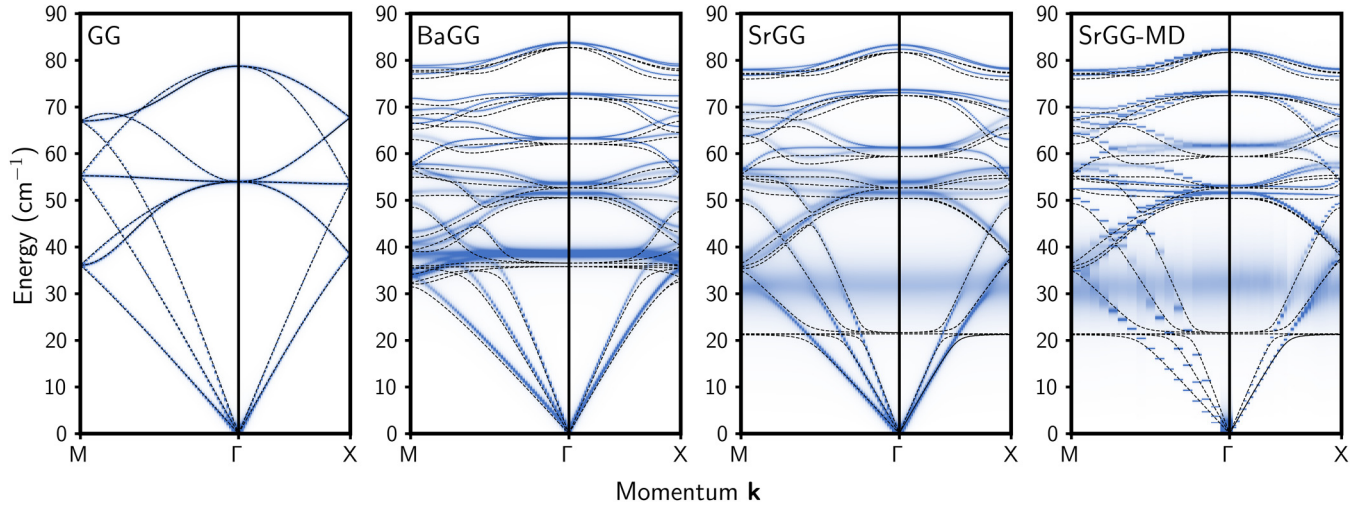


FIG. 2. Spectral functions of empty and filled clathrates at 300 K calculated using VDMFT. The rightmost panel shows the spectral function of SrGG calculated using MD with a supercell of 8192 atoms. Black dashed lines indicate the harmonic dispersion relation.

spectral functions is excellent for SrGG at 300 K, the most anharmonic system studied here. However, while MD offers limited resolution of the BZ due to the finite size of the simulated supercell, the VDMFT spectral function is accessible at all points in the BZ. Moreover, a VDMFT calculation is significantly more affordable than MD simulations: While using MD to compute the spectral function required the simulation of 8192 atoms with periodic boundary conditions, using VDMFT required the simulation of only 8 atoms coupled to a bath.

Figure 3 shows the spectral function at specific points in the BZ as well as frequency shifts and linewidths

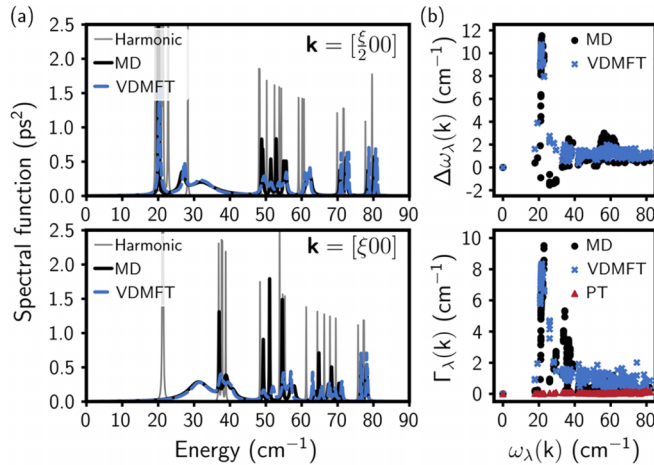


FIG. 3. (a) The spectral function of SrGG at 300 K at $\mathbf{k} = [\frac{\xi}{2}00]$ and $\mathbf{k} = [\xi00]$, where $\xi = \pi/a$, calculated using MD and VDMFT. (b) Anharmonic frequency shifts (top) and linewidths (bottom) of SrGG at 300 K obtained from the self-energy calculated using MD, VDMFT, and PT sampled on a $4 \times 4 \times 4$ grid of the BZ. The frequency shift is calculated as $\Delta\omega_\lambda(\mathbf{k}) = \omega_{\text{eff},\lambda}(\mathbf{k}) - \omega_\lambda(\mathbf{k})$, where $\omega_{\text{eff},\lambda}^2(\mathbf{k}) = \omega_\lambda^2(\mathbf{k}) + 2\omega_\lambda(\mathbf{k})\text{Re}\pi_{\lambda,\lambda}[\mathbf{k}, \omega_{\text{eff},\lambda}(\mathbf{k})]$ and was solved for iteratively. The linewidth is calculated as $\Gamma_\lambda(\mathbf{k}) = 2\omega_\lambda(\mathbf{k})\text{Im}\pi_{\lambda,\lambda}[\mathbf{k}, \omega_{\text{eff},\lambda}(\mathbf{k})]/\omega_{\text{eff},\lambda}(\mathbf{k})$.

calculated by both MD and VDMFT for SrGG at 300 K, again indicating the excellent accuracy of VDMFT in describing anharmonicity across the BZ. It is worth noting that VDMFT is accurate for various degrees of anharmonicity, capturing both the strong anharmonicity of the rattling modes as well as the nearly negligible anharmonicity of the higher-energy optical modes. Comparisons between VDMFT and MD for GG and BaGG are shown in the SM [46]. Additionally, Fig. 3(b) shows phonon linewidths computed using lowest-order PT of three-phonon scattering processes [54] (details in SM [46]). As shown in the SM, PT predicts accurate linewidths for the quasiharmonic GG, but it fails to capture any broadening for BaGG or SrGG, indicating that cage-guest anharmonicity in the filled clathrates is dominated by four- and higher-phonon scattering processes that cannot be described by PT but that are inherently included in VDMFT [46].

Next, we use our VDMFT results to better understand how anharmonicity impacts the phonon QP picture for SrGG at 300 K. To do this, we consider the diagonal approximation, which neglects nondiagonal elements of the self-energy in the phonon basis. Figure 4 shows that the SrGG spectral function computed within the diagonal approximation deviates remarkably from the full spectral function, especially where the acoustic and rattling modes intersect. These results suggest that, in addition to shifting frequencies and imparting lifetimes, anharmonicity mixes the original phonon modes, i.e., those defined by the harmonic dynamical matrix. To quantify this anharmonic mode mixing, we calculate a static and Hermitian approximation to the VDMFT self-energy, as done for example in QP self-consistent GW [55], and use it to determine the improved phonon modes for SrGG at 300 K. The right panel of Fig. 4 shows the band structure of these effective modes, which is in much better agreement with the peak positions of the fully anharmonic spectral function. In particular, the rattling mode is correctly shifted up by about 10 cm^{-1} . Through analysis of the inverse participation ratio of the QP bands, we find that cage acoustic and guest rattling modes between 25 and 35 cm^{-1} show significant mode mixing, as do modes near the BZ center that have both guest and

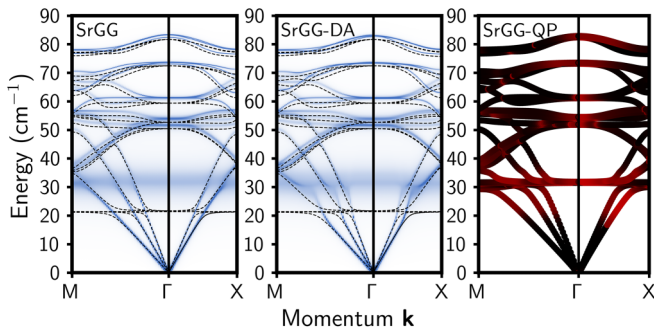


FIG. 4. The spectral functions of SrGG at 300 K calculated using the full self-energy (left), the diagonal approximation (DA, center), and the QP approximation to the full self-energy (right), where effective modes are colored according to the inverse participation ratio. Points colored in black indicate a contribution from only a single harmonic mode while points colored in red indicate the mixing of several harmonic modes.

cage character (Fig. 1). Some amount of mode mixing can also be captured by static mean-field theory, which defines a more accurate QP basis that treats both local and nonlocal anharmonicity. Such an approach can be straightforwardly combined with VDMFT [25], which would also increase its applicability to materials with longer-range anharmonicity.

IV. CONCLUSIONS

In conclusion, we have developed the methodological extensions of VDMFT for real materials, which we used to study the anharmonic lattice dynamics of clathrate solids. By comparison with exact MD simulations, we conclude that VDMFT is remarkably accurate and provides results of higher resolution at significantly lower cost. By comparison with conventional PT calculations, we find that anharmonicity in type-I clathrates is dominated by four-phonon and higher-order scattering processes, indicating that nonperturbative

effects matter. This result is applicable to a wide range of symmetric host-framework structures, including perovskites, Heusler and half-Heusler compounds, and skutterudites, suggesting the importance of nonperturbative techniques in the accurate description of anharmonicity and related material properties, such as thermal conductivities.

The VDMFT approach introduced here is completely general and can be applied to any material, although it is best suited for those with strong, local anharmonicity. While this work uses a coarse-grained classical force field, VDMFT can be straightforwardly performed with all-atom force fields or *ab initio* electronic structure theory, where the computational savings will be even more significant.

From our application to clathrate solids, we confirm that the introduction of guest atoms within the lattice framework leads to significant anharmonic effects, such as the hardening and broadening of phonon modes, that cannot be described by PT. Additionally, we find that anharmonicity changes the character of the phonon QPs via significant mixing between the X(2) rattling modes and cage acoustic modes. The impact of the strongly anharmonic rattling modes on the acoustic modes is known to have implications for thermal conductivities [31,37,38,40], which can be computed using the VDMFT GF and will be the subject of future work.

ACKNOWLEDGEMENTS

We thank P. Shih for helpful discussions. This work was supported by the U.S. Department of Energy, Office of Science, Basic Energy Sciences, under Award No. DE-SC0023002. We acknowledge computing resources from Columbia University's Shared Research Computing Facility project, which is supported by NIH Research Facility Improvement Grant No. 1G20RR030893-01, and associated funds from the New York State Empire State Development, Division of Science Technology and Innovation (NYSTAR), Contract No. C090171.

-
- [1] R. Cowley, The lattice dynamics of an anharmonic crystal, *Adv. Phys.* **12**, 421 (1963).
 - [2] N. Li, J. Ren, L. Wang, G. Zhang, P. Hänggi, and B. Li, *Colloquium: Phononics: Manipulating heat flow with electronic analogs and beyond*, *Rev. Mod. Phys.* **84**, 1045 (2012).
 - [3] M. Maldovan, Sound and heat revolutions in phononics, *Nature (London)* **503**, 209 (2013).
 - [4] X. Qian, J. Zhou, and G. Chen, Phonon-engineered extreme thermal conductivity materials, *Nat. Mater.* **20**, 1188 (2021).
 - [5] M. Först, C. Manzoni, S. Kaiser, Y. Tomioka, Y. Tokura, R. Merlin, and A. Cavalleri, Nonlinear phononics as an ultrafast route to lattice control, *Nat. Phys.* **7**, 854 (2011).
 - [6] D. J. Hooton, The use of a model in anharmonic lattice dynamics, *Philos. Mag.* **3**, 49 (1958).
 - [7] T. R. Koehler, Theory of the self-consistent harmonic approximation with application to solid neon, *Phys. Rev. Lett.* **17**, 89 (1966).
 - [8] N. Werthamer, Self-consistent phonon formulation of anharmonic lattice dynamics, *Phys. Rev. B* **1**, 572 (1970).
 - [9] M. Klein and G. Horton, The rise of self-consistent phonon theory, *J. Low Temp. Phys.* **9**, 151 (1972).
 - [10] T. Tadano and S. Tsuneyuki, First-principles lattice dynamics method for strongly anharmonic crystals, *J. Phys. Soc. Jpn.* **87**, 041015 (2018).
 - [11] P. Souvatzis, O. Eriksson, M. I. Katsnelson, and S. P. Rudin, Entropy driven stabilization of energetically unstable crystal structures explained from first principles theory, *Phys. Rev. Lett.* **100**, 095901 (2008).
 - [12] I. Errea, M. Calandra, and F. Mauri, Anharmonic free energies and phonon dispersions from the stochastic self-consistent harmonic approximation: Application to platinum and palladium hydrides, *Phys. Rev. B* **89**, 064302 (2014).
 - [13] T. Tadano and S. Tsuneyuki, Self-consistent phonon calculations of lattice dynamical properties in cubic SrTiO₃ with first-principles anharmonic force constants, *Phys. Rev. B* **92**, 054301 (2015).

- [14] S. Ehsan, M. Arrigoni, G. K. H. Madsen, P. Blaha, and A. Tröster, First-principles self-consistent phonon approach to the study of the vibrational properties and structural phase transition of BaTiO_3 , *Phys. Rev. B* **103**, 094108 (2021).
- [15] T. Tadano and W. A. Saidi, First-principles phonon quasiparticle theory applied to a strongly anharmonic halide perovskite, *Phys. Rev. Lett.* **129**, 185901 (2022).
- [16] P. G. Klemens, Anharmonic decay of optical phonons, *Phys. Rev.* **148**, 845 (1966).
- [17] L. D. Whalley, J. M. Skelton, J. M. Frost, and A. Walsh, Phonon anharmonicity, lifetimes, and thermal transport in $\text{CH}_3\text{NH}_3\text{PbI}_3$ from many-body perturbation theory, *Phys. Rev. B* **94**, 220301(R) (2016).
- [18] E. Xiao and C. A. Marianetti, Anharmonic phonon behavior via irreducible derivatives: Self-consistent perturbation theory and molecular dynamics, *Phys. Rev. B* **107**, 094303 (2023).
- [19] J. E. Turney, E. S. Landry, A. J. H. McGaughey, and C. H. Amon, Predicting phonon properties and thermal conductivity from anharmonic lattice dynamics calculations and molecular dynamics simulations, *Phys. Rev. B* **79**, 064301 (2009).
- [20] T. Sun, X. Shen, and P. B. Allen, Phonon quasiparticles and anharmonic perturbation theory tested by molecular dynamics on a model system, *Phys. Rev. B* **82**, 224304 (2010).
- [21] A. J. C. Ladd, B. Moran, and W. G. Hoover, Lattice thermal conductivity: A comparison of molecular dynamics and anharmonic lattice dynamics, *Phys. Rev. B* **34**, 5058 (1986).
- [22] O. Hellman, I. A. Abrikosov, and S. I. Simak, Lattice dynamics of anharmonic solids from first principles, *Phys. Rev. B* **84**, 180301(R) (2011).
- [23] O. Hellman, P. Steneteg, I. A. Abrikosov, and S. I. Simak, Temperature dependent effective potential method for accurate free energy calculations of solids, *Phys. Rev. B* **87**, 104111 (2013).
- [24] T. E. Markland and M. Ceriotti, Nuclear quantum effects enter the mainstream, *Nat. Rev. Chem.* **2**, 0109 (2018).
- [25] P. Shih and T. C. Berkelbach, Anharmonic lattice dynamics from vibrational dynamical mean-field theory, *Phys. Rev. B* **106**, 144307 (2022).
- [26] A. Georges and G. Kotliar, Hubbard model in infinite dimensions, *Phys. Rev. B* **45**, 6479 (1992).
- [27] A. Georges, G. Kotliar, W. Krauth, and M. J. Rozenberg, Dynamical mean-field theory of strongly correlated fermion systems and the limit of infinite dimensions, *Rev. Mod. Phys.* **68**, 13 (1996).
- [28] G. Kotliar and D. Vollhardt, Strongly correlated materials: Insights from dynamical mean-field theory, *Phys. Today* **57**(3), 53 (2004).
- [29] G. Kotliar, S. Y. Savrasov, K. Haule, V. S. Oudovenko, O. Parcollet, and C. A. Marianetti, Electronic structure calculations with dynamical mean-field theory, *Rev. Mod. Phys.* **78**, 865 (2006).
- [30] G. S. Nolas, J. L. Cohn, G. A. Slack, and S. B. Schujman, Semiconducting Ge clathrates: Promising candidates for thermoelectric applications, *Appl. Phys. Lett.* **73**, 178 (1998).
- [31] M. Christensen, A. B. Abrahamsen, N. B. Christensen, F. Juranyi, N. H. Andersen, K. Lefmann, J. Andreasson, C. R. H. Bahl, and B. B. Iversen, Avoided crossing of rattler modes in thermoelectric materials, *Nat. Mater.* **7**, 811 (2008).
- [32] J. Dong, O. F. Sankey, G. K. Ramachandran, and P. F. McMillan, Chemical trends of the rattling phonon modes in alloyed germanium clathrates, *J. Appl. Phys.* **87**, 7726 (2000).
- [33] Y. Takasu, T. Hasegawa, N. Ogita, M. Udagawa, M. A. Avila, K. Suekuni, I. Ishii, T. Suzuki, and T. Takabatake, Dynamical properties of guest ions in the type-I clathrate compounds $\text{X}_8\text{Ga}_{16}\text{Ge}_{30}$ ($X = \text{Eu}, \text{Sr}, \text{Ba}$) investigated by Raman scattering, *Phys. Rev. B* **74**, 174303 (2006).
- [34] C. H. Lee, H. Yoshizawa, M. A. Avila, I. Hase, K. Kihou, and T. Takabatake, Neutron scattering study of phonon dynamics on type-I clathrate $\text{Ba}_8\text{Ga}_{16}\text{Ge}_{30}$, *J. Phys.: Conf. Ser.* **92**, 012169 (2007).
- [35] T. Takabatake, K. Suekuni, T. Nakayama, and E. Kaneshita, Phonon-glass electron-crystal thermoelectric clathrates: Experiments and theory, *Rev. Mod. Phys.* **86**, 669 (2014).
- [36] T. Tadano, Y. Gohda, and S. Tsuneyuki, Impact of rattlers on thermal conductivity of a thermoelectric clathrate: A first-principles study, *Phys. Rev. Lett.* **114**, 095501 (2015).
- [37] T. Tadano and S. Tsuneyuki, Quartic anharmonicity of rattlers and its effect on lattice thermal conductivity of clathrates from first principles, *Phys. Rev. Lett.* **120**, 105901 (2018).
- [38] M. S. Ikeda, H. Euchner, X. Yan, P. Tomeš, A. Prokofiev, L. Prochaska, G. Lientschnig, R. Svagera, S. Hartmann, E. Gati, M. Lang, and S. Paschen, Kondo-like phonon scattering in thermoelectric clathrates, *Nat. Commun.* **10**, 887 (2019).
- [39] D. O. Lindroth, J. Brorsson, E. Fransson, F. Eriksson, A. Palmqvist, and P. Erhart, Thermal conductivity in intermetallic clathrates: A first-principles perspective, *Phys. Rev. B* **100**, 045206 (2019).
- [40] S. Godse, Y. Srivastava, and A. Jain, Anharmonic lattice dynamics and thermal transport in type-I inorganic clathrates, *J. Phys.: Condens. Matter* **34**, 145701 (2022).
- [41] M. Baggioli, B. Cui, and A. Zaccone, Theory of the phonon spectrum in host-guest crystalline solids with avoided crossing, *Phys. Rev. B* **100**, 220201(R) (2019).
- [42] S. Pailhès, V. M. Giordano, S. R. Turner, P. F. Lory, C. Candolfi, M. de Boissieu, and H. Euchner, From phonons to the thermal properties of complex thermoelectric crystals: The case of type-I clathrates, *Results Phys.* **49**, 106487 (2023).
- [43] J. Dong, O. F. Sankey, and C. W. Myles, Theoretical study of the lattice thermal conductivity in Ge framework semiconductors, *Phys. Rev. Lett.* **86**, 2361 (2001).
- [44] Q. Xi, Z. Zhang, T. Nakayama, J. Chen, J. Zhou, and B. Li, Off-center rattling triggers high-temperature thermal transport in thermoelectric clathrates: Nonperturbative approach, *Phys. Rev. B* **97**, 224308 (2018).
- [45] A. Bientien, E. Nishibori, S. Paschen, and B. B. Iversen, Crystal structures, atomic vibration, and disorder of the type-I thermoelectric clathrates $\text{Ba}_8\text{Ga}_{16}\text{Si}_{30}$, $\text{Ba}_8\text{Ga}_{16}\text{Ge}_{30}$, $\text{Ba}_8\text{In}_{16}\text{Ge}_{30}$, and $\text{Sr}_8\text{Ga}_{16}\text{Ge}_{30}$, *Phys. Rev. B* **71**, 144107 (2005).
- [46] See Supplemental Material at <http://link.aps.org/supplemental/10.1103/PhysRevB.110.064312> for details about the clathrate model and parameters; details of the VDMFT local potential, impurity problem, and fitting procedure; details of molecular dynamics and perturbation theory calculations; figures regarding temperature dependence; figures comparing VDMFT and MD calculations; and figures assessing the self-consistency of VDMFT, which includes Refs. [47–50].
- [47] S. Plimpton, Fast parallel algorithms for short-range molecular dynamics, *J. Comput. Phys.* **117**, 1 (1995).

- [48] F. Zhou, W. Nielson, Y. Xia, and V. Ozoliņš, Lattice anharmonicity and thermal conductivity from compressive sensing of first-principles calculations, *Phys. Rev. Lett.* **113**, 185501 (2014).
- [49] K. Parlinski, Z. Q. Li, and Y. Kawazoe, First-principles determination of the soft mode in cubic ZrO_2 , *Phys. Rev. Lett.* **78**, 4063 (1997).
- [50] A. A. Maradudin and A. E. Fein, Scattering of neutrons by an anharmonic crystal, *Phys. Rev.* **128**, 2589 (1962).
- [51] G. D. Mahan, *Many-Particle Physics* (Springer, Boston, 2000).
- [52] M. Ceriotti, G. Bussi, and M. Parrinello, Colored-noise Thermostats à la Carte, *J. Chem. Theory Comput.* **6**, 1170 (2010).
- [53] M. Ceriotti and M. Parrinello, The δ -thermostat: Selective normal-modes excitation by colored-noise Langevin dynamics, *Procedia Comput. Sci.* **1**, 1607 (2010).
- [54] T. Tadano, Y. Gohda, and S. Tsuneyuki, Anharmonic force constants extracted from first-principles molecular dynamics: Applications to heat transfer simulations, *J. Phys.: Condens. Matter* **26**, 225402 (2014).
- [55] M. van Schilfgaarde, T. Kotani, and S. Faleev, Quasiparticle self-consistent *GW* theory, *Phys. Rev. Lett.* **96**, 226402 (2006).